Supplementary Information (SI) for Energy & Environmental Science.
This journal is © The Royal Society of Chemistry 2026

Supplementary Information

Bingsen Wang, Nan He, Yupeng Bai, Pengpeng Miao, Yu Li, Haonan Wang*, Xingsen Mu, Dawei Tang, Yongchen Song*, Lin Li*

Key Laboratory of Ocean Energy Utilization and Energy Conservation of Ministry of Education, School of energy and power engineering, Dalian University of Technology; Dalian, 116024, P. R. China.
*Corresponding author. Email: wanghaonan@dlut.edu.cn (Haonan Wang), songyc@dlut.edu.cn (Yongchen Song), lilinnd@dlut.edu.cn (Lin Li)

Supplementary Text

Synthesis of PANI (Polyaniline) hydrogel electrode: The PANI hydrogel electrode layer was synthesized following the procedure reported in our previous work (*40*). Briefly, an initial solution was formulated by dissolving 0.362 g N-isopropylacrylamide (NIPAM), 100 mg of PANI, 20 mg of sodium dodecyl sulfate (SDS), N, N'-methylenebisacrylamide (MBAA, 5% mol of NIPAM), and 14 μL of acrylic acid in 14.5 mL of deionized (DI) water. Subsequently, the solution was subjected to a 30-minute N_2 bubbling process to eradicate any residual oxygen present. Following this, the solution was heated to 75℃, and 0.5 ml (8.6 g L^{-1} in DI water) potassium persulfate (KPS) solution was added. The solution was then agitated for 2 hours at 75℃. Finally, after the solution was slowly cooled to room temperature, dialysis bags (3500 nominal MWCO, MD44, China) were used to remove the unreacted monomers in the solution to obtain ionic microgel dispersion. The dialysis was conducted in DI water for 2 days, with the water being replaced every 6 hours. Then, 8 ml initial solution dispersion with initial solid content, 2 g acrylamide (AM), 4 mg MBAA, 100 mg KPS and SDS (0.5% mol of AM) were mixed. After 30 minute of stirring, the obtained mixture solution was placed into the appropriate Teflon mold, which was then heated overnight at 50°C. The final obtained PANI layer were ready for further synthesis.

This approach effectively reduces the Young's modulus (**Fig. S3**) while maintaining the intrinsic electrical conductivity of PANI, offering greater softness than direct PANI doping within the hydrogel and thereby enabling flexible encapsulation.

Calculation of energy conversion efficiency and total power output of the EVS-MEG: First, we have calculated the energy conversion efficiency of the EVS-MEG using Equation 1 reported in the authoritative reference [1] in the field of moisture-enabled power generation. The energy conversion efficiency (η) can be described by the following equation:

$$\eta = \frac{E_{\text{output}}}{\Delta H_{\text{gas}} - \Delta H_{\text{absorbed}}} \qquad \text{* MERGEFORMAT (1)}$$

where E_{output} represents the specific output energy of water during the water sorption process. The ΔH_{gas} and $\Delta H_{absorbed}$ represent the enthalpies of formations of gaseous water in moisture and sorbed water in sorbents, respectively. ($\Delta H_{\text{gas}} - \Delta H_{absorbed}$) represents the total energy changes during the water sorption process. [1]

In the practical calculation, the ambient temperature was taken as T=298.15 K, the relative humidity was 80%, and the pressure was approximated as standard atmospheric pressure: P=0.101325 MPa. During the moisture-absorption process, the temperature variation at the surface of the EVS-MEG can be neglected; therefore, this process can be reasonably approximated as an isothermal phase-change process. Using t=1 s as the time interval, the electrical energy output E_{output} was defined as the energy delivered per unit area by the EVS-MEG operating at its peak output power P_{max} within t. The total input energy was taken as the phase-change energy associated with the absorbed moisture mass (m) per unit area during the t. Accordingly, equation 1 can be further rewritten as equation 2:

$$\eta = \frac{P_{\text{max}} \times t}{m\,(\Delta h^{0}_{\text{gas}} - \Delta h^{0}_{\text{liquid}})} \qquad \text{* MERGEFORMAT (2)}$$

where P_{max}=65.3 μW cm^{-2}, m=3.93 μg was determined by the experiment. The enthalpy change value was 2442 J g^{-1}.[1] So, the energy conversion efficiency (η) of the EVS-MEG was calculated to be about **0.68%**.

We evaluated the power output capability of the EVS-MEG over its entire lifetime based on the classical theory (equation 3) [2] and the derived equation 4:

$$P_{\text{t-max}} = \frac{1}{4} V_{\text{OC}} I_{\text{SC}} \qquad \text{* MERGEFORMAT (3)}$$

$$E_t = \frac{1}{4}\int_0^t V_{\text{OC}} I_{\text{SC}}\, \mathrm{d}t \qquad \text{* MERGEFORMAT (4)}$$

where $P_{\text{t-max}}$ represents the theoretical maximum power, V_{oc} and I_{sc} represent the open-

circuit voltage and short-circuit current of MEG, respectively, and E_t represents the theoretical electrical energy output during t. After calculation, the energy output of a 1 cm^2 EVS-MEG over a t=500 hours lifetime was $\boldsymbol{E_t}$**=225.432 J**.

It should be emphasized that this value represents only a theoretical estimate of the maximum energy output. Considering the fluctuations of the external load resistance in the circuit and the presence of electrode contact impedance, the actual output is expected to be lower. [3]

Synthesis of control groups: For comparison, PAM-LiCl hydrogel and other control groups were synthesized using the following method:

To prepare the PAM-LiCl hydrogels, 2 g of AM, 1.5 g of LiCl, 0.0086 g of 2-hydroxy-4'-(2-hydroxyethoxy)-2-methylpropiophenone (HHM) and 0.0028 g of MBAA were dissolved in 7 mL of DI. The mixture was then stirred on a magnetic stirrer for 30 minutes until the clear solution was obtained. The clear hydrogel precursor solution was poured into the polytetrafluoroethylene mold and subjected to ultraviolet irradiation at 365 nm with a power of 45 W for 40 minutes to complete the polymerization reaction.

To prepare the PAM-Gly-LiCl hydrogels, 2 g of AM, 1.5 g of LiCl, 0.0086 g of HHM and 0.0028 g of MBAA were dissolved in a mixed solvent of 4 mL of DI and 3.78 g of (glycerol) Gly. The mixture was then stirred on a magnetic stirrer for 30 minutes until the clear solution was obtained. The photopolymerization step of the precursor solution is same as described above.

To prepare the PAM-AMPS-Gly-LiCl hydrogels, 2 g of AM, 1.5 g of 2-acrylamido-2-methylpropanesulfonic acid (AMPS), equal n(AM) of lithium polyacrylate, 0.0086 g of HHM and 0.0028 g of MBAA were dissolved in a mixed solvent of 4 mL of DI and 3.78 g of Gly. The mixture was then stirred on a magnetic stirrer for 30 minutes until the clear solution was obtained. The photopolymerization step of the precursor solution is same as described above.

To prepare the ionic hydrogel with different n (LiCl: supermolecule), 2 g of AM, 0.0028 g of MBAA, 0.0086 g of HHM, 1.5g of AMPS and different components (0 n(AM) of lithium polyacrylate with equal n (AM) of LiCl; 0.25 n(AM) of lithium polyacrylate with 0.75 n (AM) of LiCl; 0.5 n(AM) of lithium polyacrylate with 0.5 n (AM) of LiCl; 0.75 n(AM) of lithium polyacrylate with 0.25 n (AM) of LiCl; equal n(AM) of lithium polyacrylate with 0 n (AM) of LiCl) were dissolved in a mixed solvent of 4 mL of DI and 3.78 g of Gly. The mixture was then stirred on a magnetic stirrer for 30 minutes until the clear solution was obtained. The photopolymerization step of the precursor solution is same as described above.

To prepare the PAM-LiCl-(TM-β-CD) hydrogels: 2 g of AM, 1.5 g LiCl, 0.3g TM-β-CD (Heptakis (2,3,6-tri-O-methyl)-β-cyclodextrin), 0.0086 g of HHM and 0.0028 g of MBAA were dissolved in a mixed solvent of 7 mL of DI water. The mixture was then stirred on a magnetic stirrer for 30 minutes until the clear solution was obtained. The photopolymerization step of the precursor solution is same as described above.

To prepare the PVA-gly-NaCl hydrogels: 1g PVA, 2g NaCl, 2g glycerol were dissolved in 8 mL DI water and then heat and stirred at 90℃ until all the solute is completely dissolved. After the mixed solution cools down to 50℃, slowly added 50 μL of glutaraldehyde and 0.1 ml of 1 mol/L hydrochloric acid during Stirring. Then the mixed solution was poured into the mold. Place it at room temperature overnight to obtain the final hydrogels.

To prepare the PVA-gly-PAACNa hydrogels: 1g PVA, 3.2g PAACNa solution (50% in water), 2g glycerol were dissolved in 6.4 mL DI water and then heat and stirred at 90℃ until all the solute is completely dissolved. After the mixed solution cools down to 50℃, slowly added 50 μL of glutaraldehyde and 0.1 ml of 1 mol/L hydrochloric acid during Stirring. Then the mixed solution was poured into the mold. Place it at room temperature overnight to obtain the final hydrogels.

The recovery mechanism of the Li^+ concentration and water gradient in EVS-MEG: The Li^+ concentration gradient and water gradient in the EVS-MEG can be restored by directional heating at 80°C to evaporate water from the hydrogel. Before

heating, the bottom and side surfaces of the EVS-MEG are sealed with plastic film, leaving only the top surface exposed to air. During heating, the top surface dries first, while the bottom remains relatively hydrated, thereby establishing a moisture gradient from the bottom to the top. The higher degree of Li^+ dissociation at the bottom consequently generates an upward ion concentration gradient. In addition, a portion of the anions in the EVS-MEG exists as polymer-bound groups (such as $-COO^-$). Due to their large size and slow diffusion kinetics, [4] leads to the accumulation of Li^+ in the bottom during the discharge process. After the discharge process ends and the external electric field is removed, the electrostatic interaction generated by the accumulated anionic groups drives Li^+ in the opposite direction. In summary, these two factors jointly promote the upward migration of Li^+ toward the top of the EVS-MEG, thereby gradually restoring the initial ion concentration.

Photocurrent response characteristics of EVS-MEGs

The introduction of a PANI electrode layer for encapsulating the MEG enables further enhancement of the current output performance of the EVS-MEG under illumination. This improvement arises from the intrinsic photoelectric properties of PANI. Owing to its unique conjugated π-electron system (**Fig. S8a**), PANI can absorb light in the 400-800 nm wavelength range, where π electrons are excited from the HOMO level to the LUMO, generating electron-hole pairs [5]. Since light irradiation only excites electrons without inducing additional ionic ionization, [6] it primarily enhances the current output of the MEG, while exerting a limited effect on voltage amplification. This phenomenon is corroborated by the current-voltage characterization results (Fig. S8c).

In the absence of the EVS structure, a pure PANI hydrogel film generates a photoinduced current of only about 2 μA cm^{-2} under 1 sun illumination, accompanied by pronounced fluctuations (Fig. S8b), likely due to the random motion of free electrons. In contrast, the EVS-MEG structure produces a significant current enhancement exceeding 0.5 mA under the same illumination conditions. This enhancement can be attributed to the protonation doping of Li^+ in PANI (Fig. S8c)

and the directional migration of photoexcited electrons driven by the electric field generated within the EVS-hydrogel. As a result, the EVS-MEG achieves a maximum current density of 1.06 mA cm^{-2} under 1 sun.

Furthermore, the moisture-electric generation performance of the EVS-MEG was evaluated under natural sunlight in various weather conditions (sunny and cloudy), as shown in Fig. S8d. With increasing light intensity, the current output of the EVS-MEG increased correspondingly. Even under low-irradiance cloudy conditions, the device maintained a current output of approximately 0.65 mA cm^{-2}, demonstrating its strong potential for real-world applications.

Signal sensing and human-machine interaction experiments: In this study, the commercial physiological signal detection sensor employed for testing was purchased from Taobao (model: BMD101), with nominal operating parameters of 5.5 V and 0.6 mA. An array consisting of 24 EVS-MEG units (2 cm × 1 cm) connected in a series-parallel configuration provided sufficient power for device operation. The EVS-MEG units were connected by flexible conductive carbon tapes, and the circuit connections were strengthened by conductive carbon paste. All the EVS-MEG units were integrated on a flexible PET (polyethylene terephthalate) substrate. The acquired data were transmitted via a TTL-USB communication bus and recorded using the commercial software *sscom32.exe*.

For the human-machine interaction experiments, the experimental setup comprised 9 EVS-MEG units (1 cm × 1 cm), each independently connected to a data acquisition module. EVS-MEG units are integrated together through flexible circuits. The flexible circuit was made by changxingkuaijie, Shenzhen, China. To ensure the safety of the volunteers, external resistors were incorporated during operation to constrain the output current within the microampere (μA) range (**Fig. S9**). The volunteers participating in the electrocardiogram and blood pressure signal measurements, as well as in the human-machine interaction experiments, were the authors of this work, who provided informed consent prior to testing. The experiments involved no health risks to the volunteers and did not require approval from an institutional ethics committee.

Statistical analysis: All the experimental data in column charts were collected from various samples, with results presented as mean ± standard deviation (s. d.) and a sample size of $n \geq 3$. All the data analysis was performed using Microsoft Excel and Origin 2018 software.

Supplementary Figures

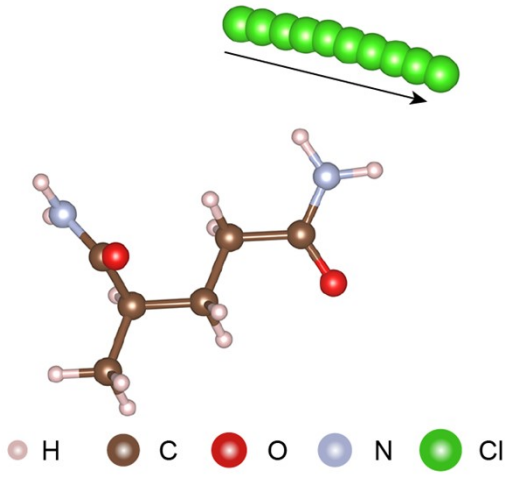

Fig. S1. Optimized structure of chloride ion diffusion in PAM-LiCl hydrogel.

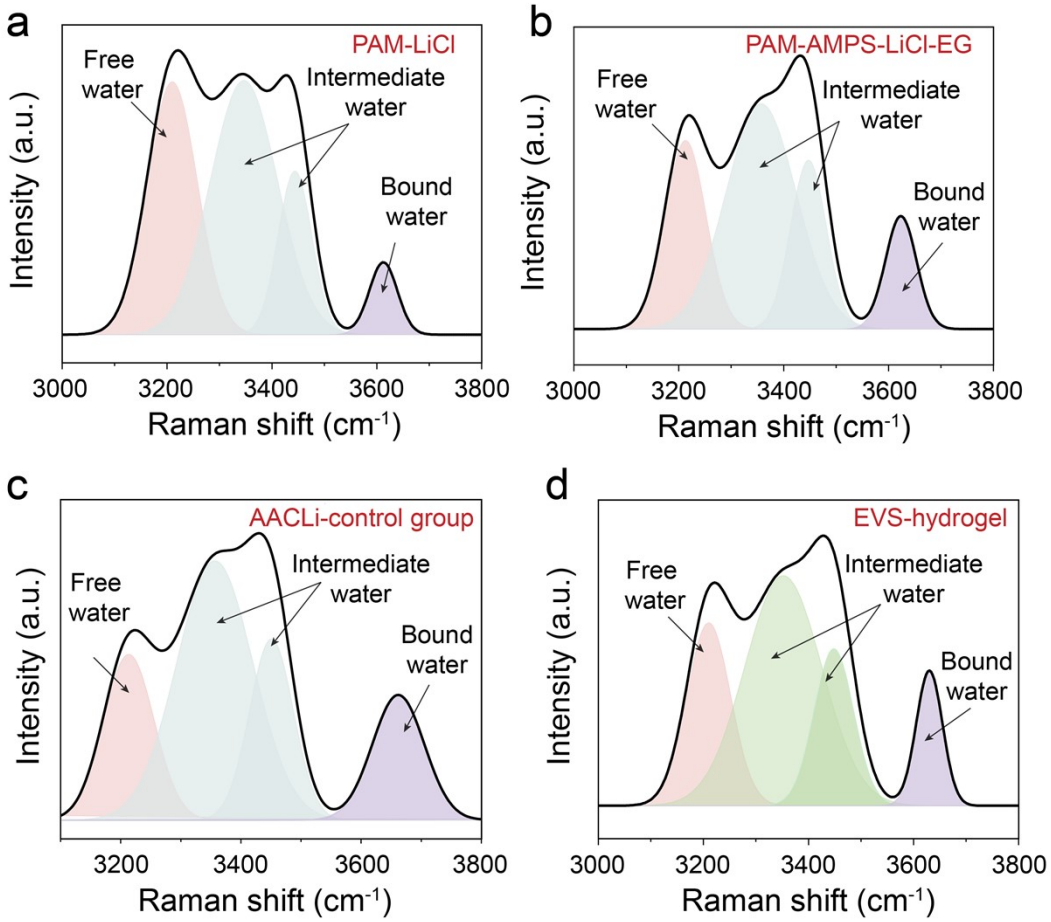

Fig. S2. Raman spectrum of the hydrogels with different contents of supramolecular structure.

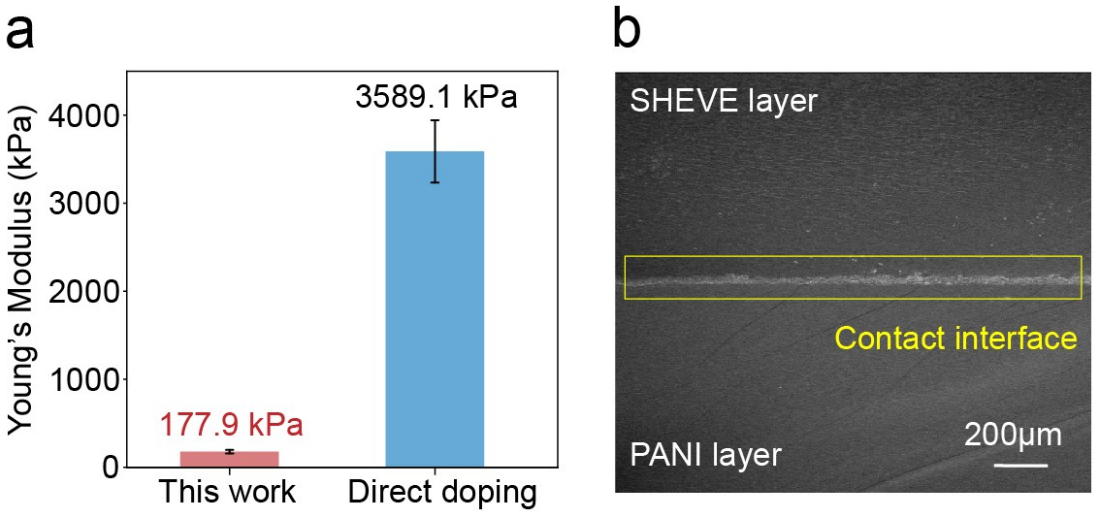

Fig. S3. **a** Young's modulus of PANI hydrogel layers prepared by different methods. The Young's modulus of the PANI hydrogel electrode synthesized by the microgel strategy is one order of magnitude lower than that of the directly doped PANI hydrogel. **b** SEM images of EVS-hydrogel and PANI electrode layer. It indicates that the two layers are in close contact with each other, which is beneficial for reducing the contact resistance.

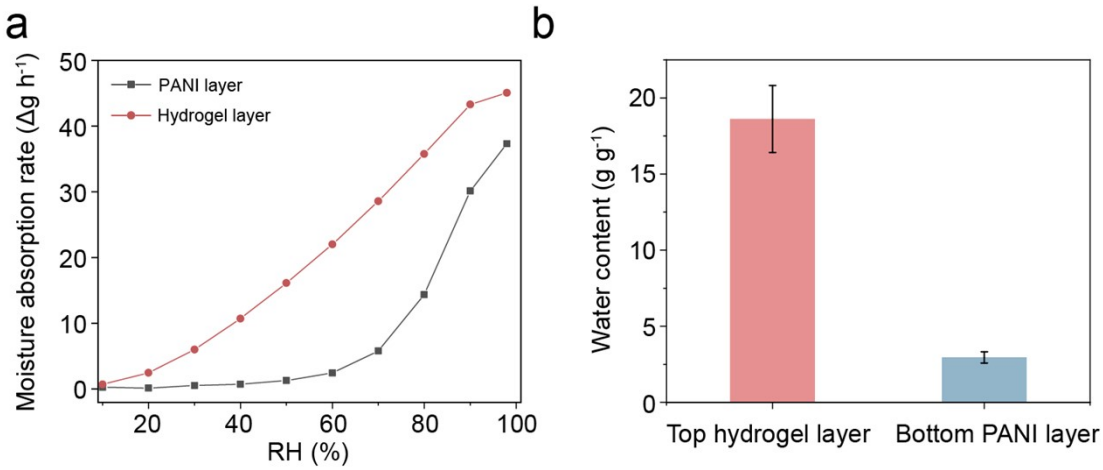

Fig. S4. Moisture absorption rate (a) and saturated water content (b) of the top EVS-hydrogel layer and the bottom PANI electrode layer.

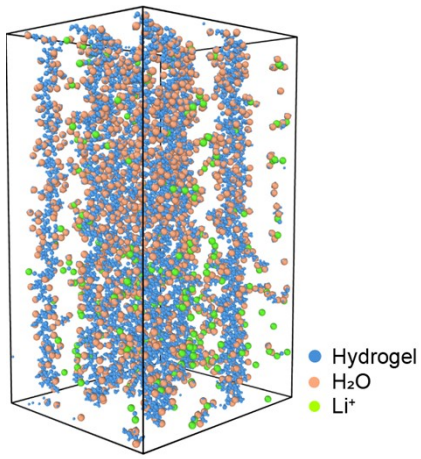

Fig. S5. Molecular configuration of PAM-LiCl hydrogel in molecular dynamic simulations.

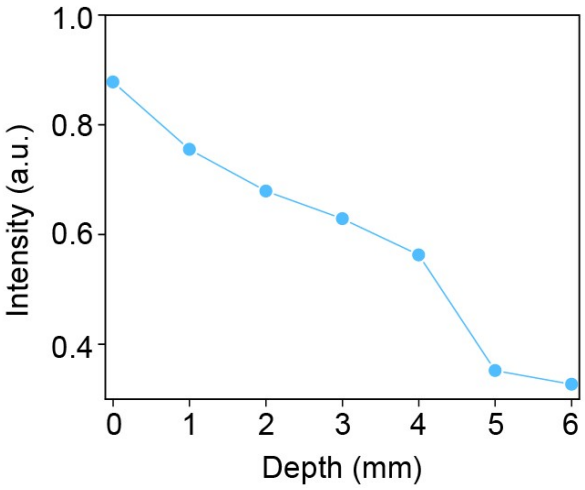

Fig. S6. The normalized Raman band ratio of O-H/C-H bond changes with the depth. The C-H bonds of stretching vibration area are within 2800-3000 cm^{-1} and O-H bonds of stretching vibration area are within 3050-3650 cm^{-1}.[7]

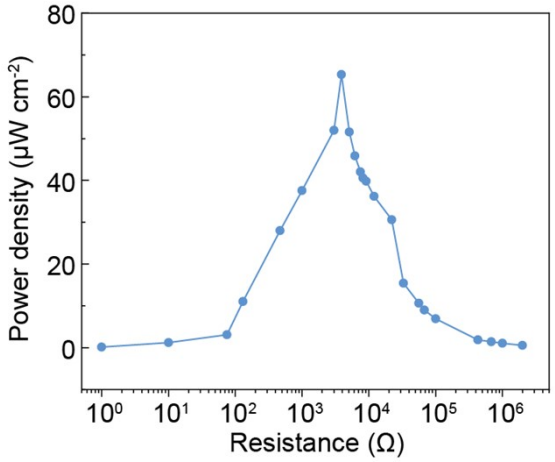

Fig. S7. The output power density with external resistance varied from 1 Ω to 2×10^6 Ω at 80%RH.

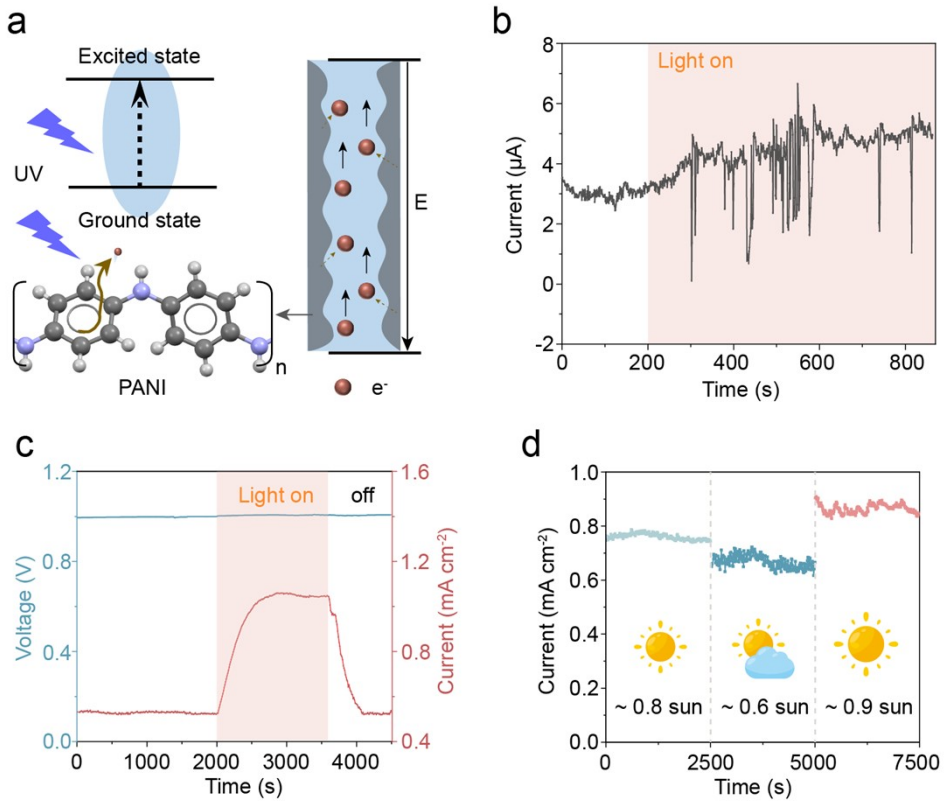

Fig. S8. **a** Schematic diagram of the photoelectric current effect of PANI. **b** Current excitation performance of PANI electrode layer under 1 sun illumination. **c** Photoexcited current-voltage characteristics of EVS-MEGs under 1 sun illumination. **d** Photoexcited short-circuit current in the natural environment.

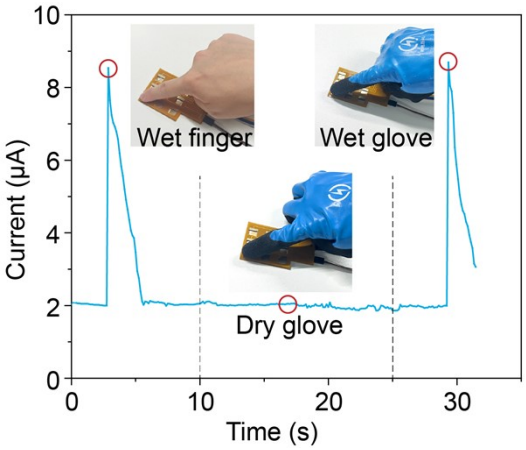

Fig. S9. The current excitation performance of the EVS-MEGs array when wearing dry insulating rubber gloves, wet insulating rubber gloves, and without gloves.

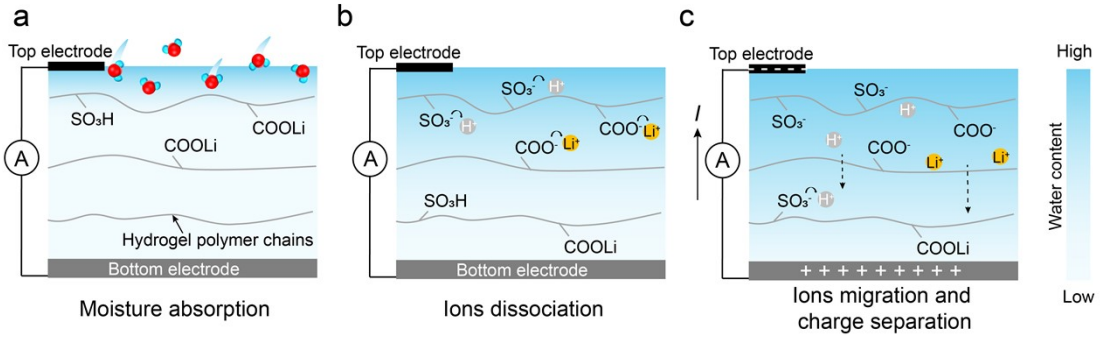

Fig. S10 Schematic of the moisture-enabled power-generation mechanism of the hydrogel MEGs.

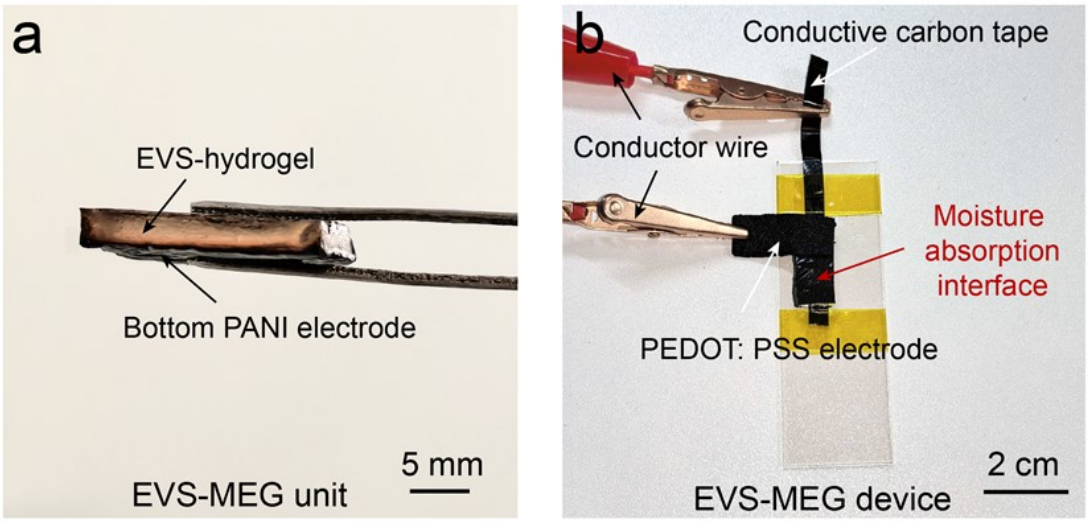

Fig. S11 a The side view of an EVS-MEG unit. **b** Photo of an EVS-MEG device.

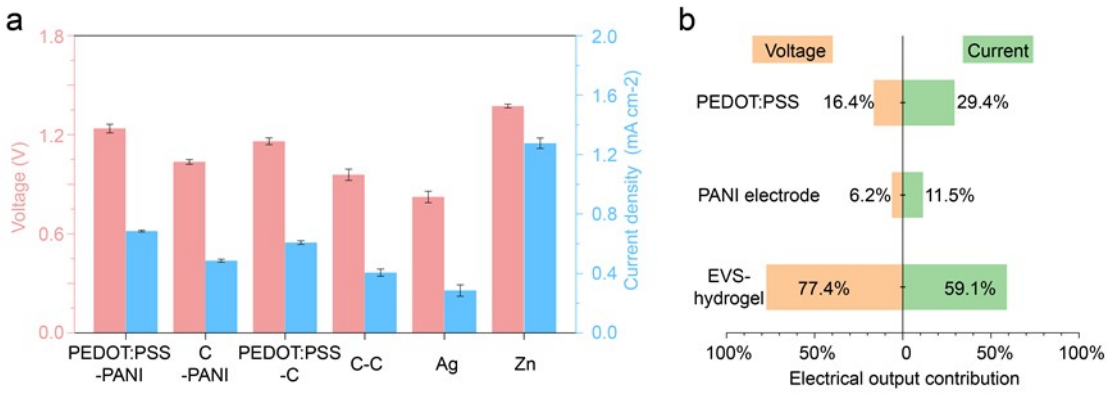

Fig. S12 a The electrical output of the EVS-MEG with different electrodes (25℃, 80%RH). b Comparison of the contribution to the electrical output performance of EVS-MEG from asymmetric wettability structures and asymmetric electric field.

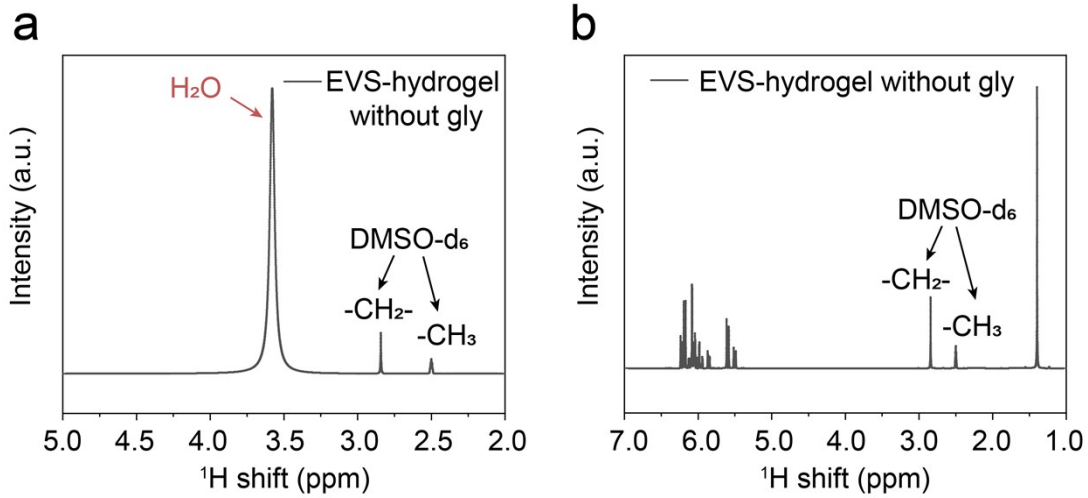

Fig. S13 a ^{1}H NMR spectrum of the EVS-hydrogel without glycerol (gly). **b** Water suppressed ^{1}H NMR spectra of the EVS-hydrogel without gly. The water peak located at 3.5-4.0 ppm exhibits a well-defined single-peak feature, similar to that observed for PAM-LiCl hydrogel. The water-suppressed ^{1}H NMR spectrum of the same sample measured under identical conditions confirms that the peak between 3.5 and 4.0 ppm corresponds to the water signal.

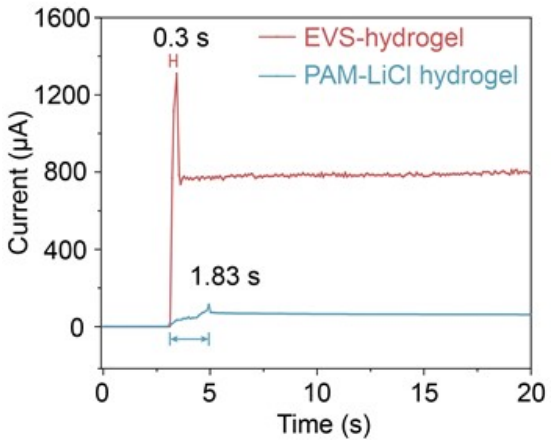

Fig. S14 Current excitation characteristics of the hydrogel upon contact with water (80%RH).

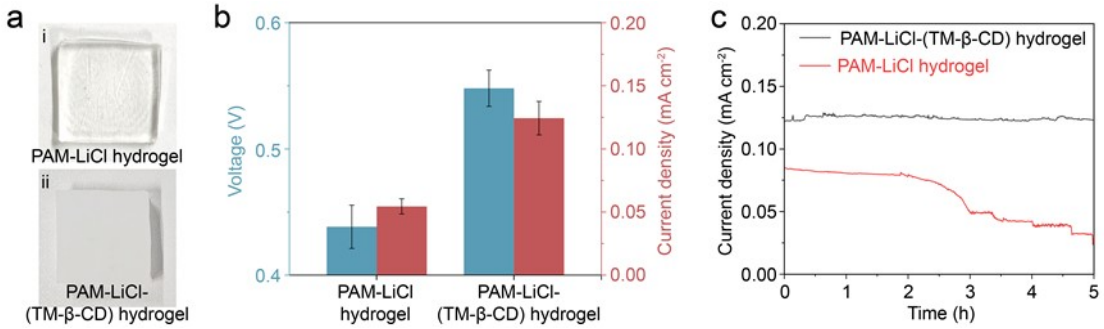

Fig. S15 a Photograph of the hydrogels**. b** Open-circuit voltage and short-circuit current output performance of the PAM-LiCl hydrogel MEG and the PAM-LiCl-(TM-β-CD) hydrogel MEG under 40% RH. Inert conductive carbon tape electrodes were used as both the top and bottom electrodes for performance testing.

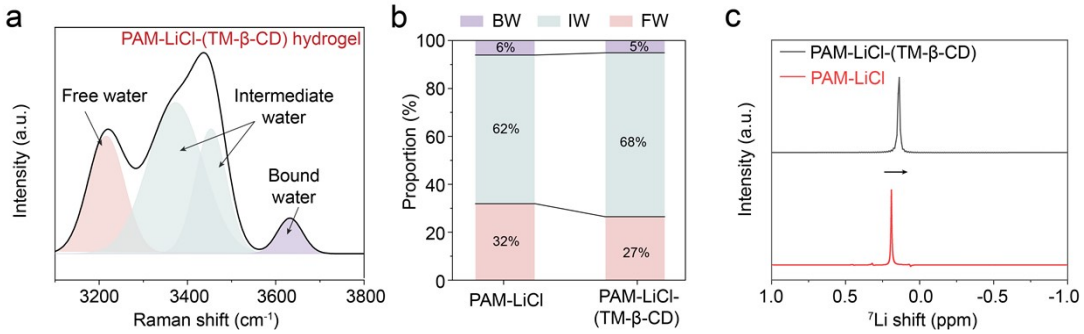

Fig. S16 a Raman spectrum of PAM-LiCl-(TM-β-CD) hydrogel. **b** Proportions of bound water (BW), intermediate water (IW), and free water (FW) in different hydrogels based on the Raman spectra analysis. **c** Normalized ^{7}Li NMR spectra of PAM-LiCl hydrogel and PAM-LiCl-(TM-β-CD) hydrogel. ^{7}Li shifts downfield upon introducing the TM-β-CD, leading to enhanced ion dissociation. [8]

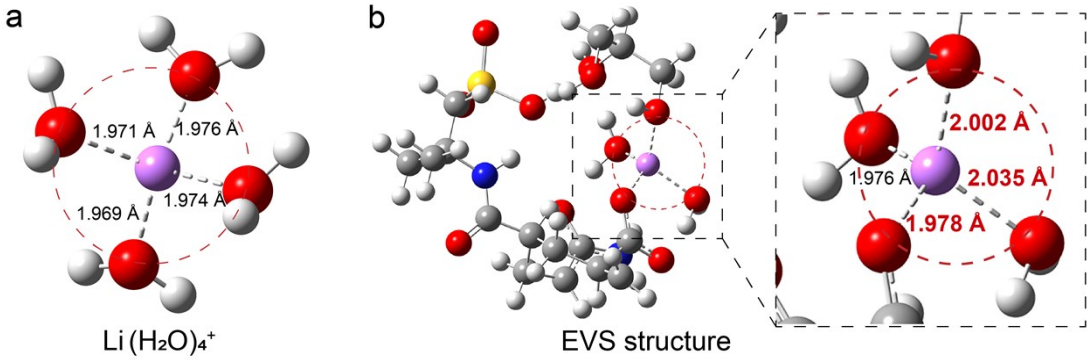

Fig. S17 a The Li-O_{water} length in the typical Li $(H2O)_4^+$ structure. **b** The Li-O_{water} length in the EVS structure. DFT calculations were performed with the Gaussian 16 and Gauss View 6.0.16 suite of programs. The structure of Li $(H2O)_4^+$ and EVS were optimized at the B3LYP/6-31G (d, p) level and then calculated at the M062X/def2TZVP level.

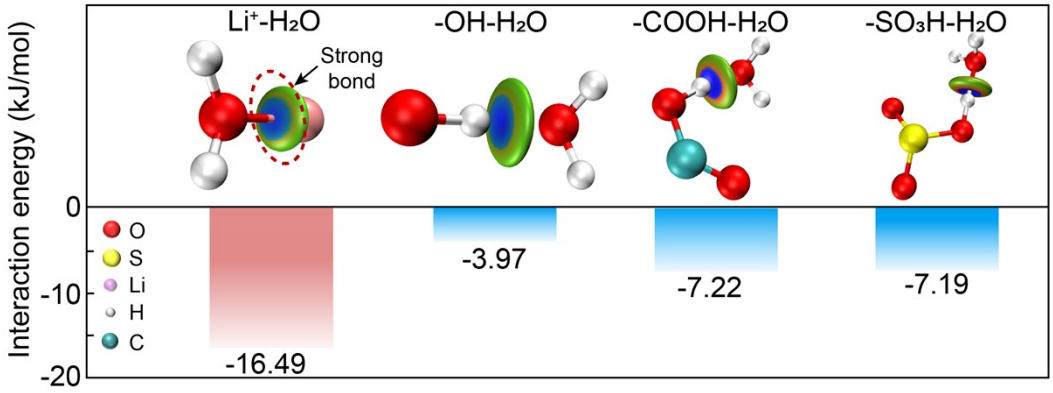

Fig. S18 The interaction energy between H_2O and Li^+, H_2O and -OH, H_2O and -COOH, as well as H_2O and $-SO_3H$. DFT calculations were performed with the Gaussian 16 and Gauss View 6.0.16 suite of programs. The structures were optimized at the B3LYP/6-31G (d, p) level and then calculated at the M062X/def2TZVP level.

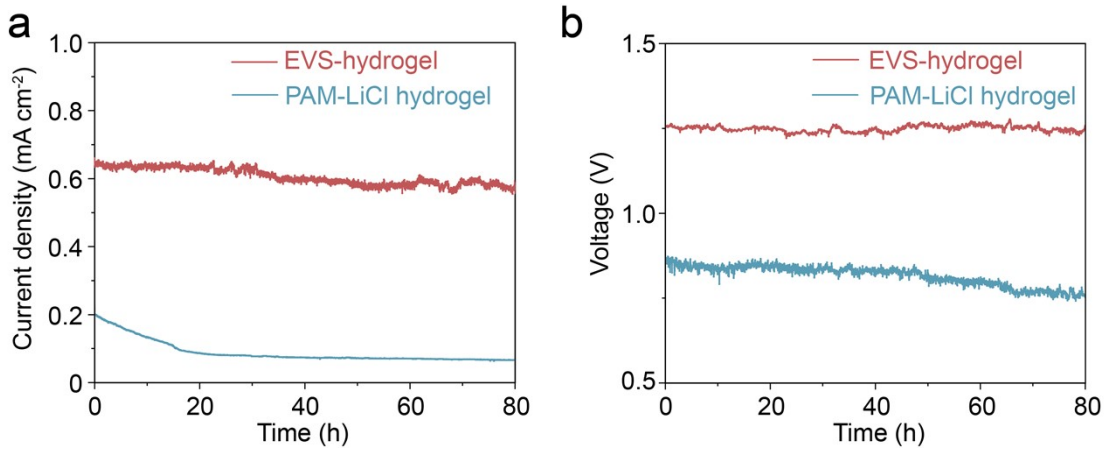

Fig. S19 The open-circuit voltage and short-circuit current output performance of **a** the EVS-hydrogel and **b** the PAM-LiCl hydrogel during 80 hours. (25°C, 80% RH). After 80 hours of continuous discharge, the current density and voltage of the control group decreased by 61% and 13%, respectively. In contrast, the EVS-MEG maintained stable output, with current density and voltage decreasing by only 10% and 2%, respectively.

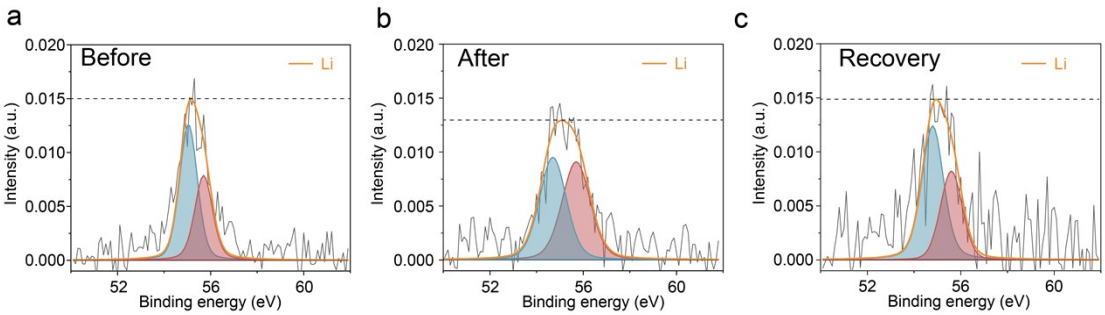

Fig. S20 Normalized Li XPS spectra of EVS-hydrogel **a** before discharge, **b** after 7 days of discharge, and **c** after drying at 80°C for 24 hours. After 7 days of continuous discharge, a significant decrease in Li^+ content in the EVS-hydrogel was observed, which can be attributed to directional ion migration. After directional drying at 80°C for 24 h, the Li^+ content nearly returned to its initial value, demonstrating the recoverability of the ion concentration gradient in the EVS-hydrogel.

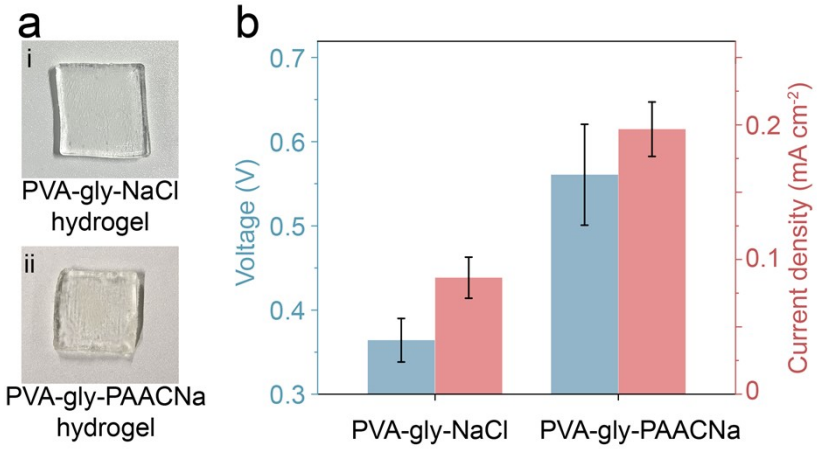

Fig. S21 a Photograph of the hydrogels**. b** Open-circuit voltage and short-circuit current output performance of the PVA-gly-NaCl hydrogel and the PVA-gly-PAACNa hydrogel under 40% RH.

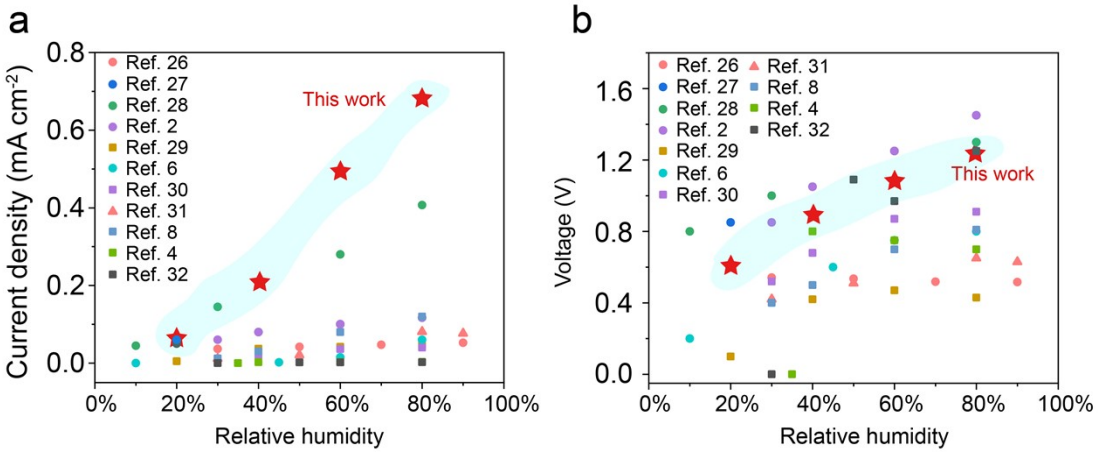

Fig. S22 Comparison of **a** the short-circuit current performance and **b** the open-circuit voltage performance representative references with our work under different relative humidity. [9-19]

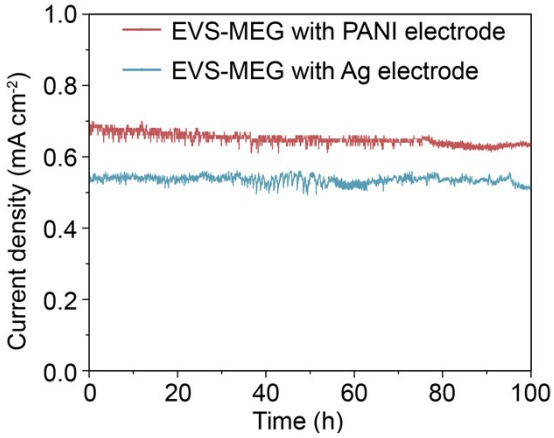

Fig. S23 Long-term short-circuit current output performance of the EVS-MEG with different bottom electrodes under 80% RH, 25℃. The top electrode was fixed as a PEDOT: PSS-graphite felt electrode.

References

1. J. Xu, P. Wang, Z. Bai, H. Cheng, R. Wang, L. Qu and T. Li, *Nature Reviews Materials*, 2024, **9**, 722-737.

2. C. Fu, X. Lu and T. Yang, *Journal of Physics D: Applied Physics*, 2024, **57**, 373003.

3. L. Yang, L. Gan, Z. Zhang, Z. Zhang, H. Yang, Y. Zhang and J. Wu, *ACS Omega*, 2022, **7**, 13906-13912.

4. N. He, H. Wang, F. Li, B. Jiang, D. Tang and L. Li, *Energy & Environmental Science*, 2023, **16**, 2494-2504.

5. Nešpůrek S., *Czech. J. Phys.* 1973, **23**, 368–390.

6. De Albuquerque, J.E., Melo, W.L.B. and Faria, R.M. *J. Polym. Sci. B Polym. Phys.*, 2000, **38**, 1294-1300.

7. Yang, S., Zhang, L., Mao, J. et al. *Nature Communications.* 2024, **15**, 3329.

8. J. Chen, Y. Gao, L. Shi, W. Yu, Z. Sun, Y. Zhou, S. Liu, H. Mao, D. Zhang, T. Lu, Q. Chen, D. Yu and S. Ding, *Nature Communications*, 2022, **13**, 4868.

9. E. Shin, G. Kim, K. Zhao, G. Zan, H. Kim, S. Li, J. Lee, D. Kang, J. W. Oh, J. Jung, J. K. Shim and C. Park, *Energy & Environmental Science*, 2024, **17**, 7165-7181.

10. X. Zhang, Z. Dai, J. Chen, X. Chen, X. Lin, S. Yang, K. Wu, Q. Fu and H. Deng, *Energy & Environmental Science*, 2023, **16**, 3600-3611.

11. S. Yang, L. Zhang, J. Mao, J. Guo, Y. Chai, J. Hao, W. Chen and X. Tao, *Nature Communications*, 2024, **15**, 3329.

12. J. Bai, Q. Liao, H. Yao, T. Guang, T. He, H. Cheng and L. Qu, *Energy & Environmental Science*, 2023, **16**, 3088-3097.

13. S. Guo, Y. Zhang, Z. Yu, M. Dai, X. Liu, H. Wang, S. Liu, J. J. Koh, W. Sun, Y. Feng, Y. Chen, L. Yang, P. Sun, G. Lu, C. Yu, W. Chen, S. De Wolf, Z. Wang and S. C. Tan, *Nature Communications*, 2025, **16**, 5267.

14. S. Yang, X. Tao, W. Chen, J. Mao, H. Luo, S. Lin, L. Zhang and J. Hao, *Advanced Materials*, 2022, **34**, 2200693.

15. C. Guo, H. Tang, D. Kong, Q. Chen, X. Wu, F. Fan, X. Zhao, R. Ding, W. Zhong and D. Zhao, *Energy & Environmental Science*, 2026, **19**, 230-240.

16. F. Yu, Y. Zhang, L. Wang, X. Yang, Y. Yang, X. Li, Y. Gao, X. Zhang, W. Lü, K. Jiang, X. Sun and D. Li, *Advanced Materials*, 2026, **38**, e09043.

17. H. Zhang, N. He, B. Wang, B. Ding, B. Jiang, D. Tang and L. Li, *Advanced Materials*, 2023, **35**, 2300398.

18. Z. Sun, X. Wen, L. Wang, J. Yu and X. Qin, *Energy & Environmental Science*,

2022, **15**, 4584-4591.
19. J. Zhou, Z. Ren, X. Cui, X. Liu and X. Lu, *Advanced Energy Materials*, 2025, **15**, 2404840.